Applied Catalysis B: Environmental 160–161 (2014) 621–628

Contents lists available at ScienceDirect

Applied Catalysis B: Environmental

journal homepage: www.elsevier.com/locate/apcatb

Enhanced photocatalytic performance of TiO_2 based on synergistic effect of Ti^{3+} self-doping and slow light effect

Dianyu Qi [a], Liujia Lu [a], Zhenhao Xi [a], Lingzhi Wang [a,*], Jinlong Zhang [a,b,**]

[a] Key Laboratory for Advanced Materials and Institute of Fine Chemicals, East China University of Science and Technology, 130 Meilong Road, Shanghai 200237, PR China
[b] Department of Chemistry, Tsinghua University, Beijing 100084, PR China

ARTICLE INFO

Article history:
Received 16 April 2014
Received in revised form 10 June 2014
Accepted 13 June 2014
Available online 20 June 2014

Keywords:
TiO_2
Inverse opal, Ti^{3+}
Oxygen vacancy
Slow light

ABSTRACT

A range of TiO_2 inverse opals with tunable macroporous size were synthesized using different sized PS (polystyrene sphere) arrays as hard templates. After a simple heating treatment in vacuum, Ti^{3+} doped TiO_2 inverse opals were obtained. The materials were characterized and verified by XRD, XPS, UV–vis DRS, EPR, and SEM. The result indicated that the optical responses of TiO_2 and Ti^{3+} doped TiO_2 inverse opals could be enhanced by choosing PS arrays with appropriate size as hard templates due to the slow light effect of inverse opal structure. The photocatalytic efficiency was evaluated by the photo degradation of AO7, and it is proved that the cooperation of slow light effect and Ti^{3+} doping is an effective way to improve visible-light driven photocatalytic performance of TiO_2 photocatalyst.

1. Introduction

TiO_2 as non-toxic, stable, low cost and high efficient photocatalyst, has attracted much attention in photocatalysis chemistry over past several decades [1]. But the band gap of titania is so wide that it only absorbs ultraviolet light, which accounts for just 4% of solar irradiation. To overcome this problem, versatile strategies based on physical or chemical methods have been applied to harvest more light irradiations and extend the optical response range of TiO_2 [2–7].

A new way based on physical concept to increase the light harvesting ability of TiO_2 has been successfully provided by photonic crystal, which is a periodic structure with photonic stop band, meaning that the propagation of light at certain wavelength is forbidden [8]. In photonic crystal, slow light effect can be observed [9], which means the light near its photonic stop band edges undergoes multiple scattering and travel with very low group velocity. As a result, the light near the photonic stop band is largely absorbed due to the slow light effect. Inverse opal is a typical photonic crystal with periodic macropores, and its photonic stop band can be controlled by adjusting the pore size of macropores. Thus, the slow light effect of inverse opal has been widely applied to improve the intrinsic optical response of the material for improving its photochemical performance [10]. For example, Ozin and co-workers [11] prepared a range of TiO_2 inverse opals with different photonic stop bands and found that the photocatalytic activity of TiO_2 could be largely enhanced when photonic stop band is close to the electronic band gap of the TiO_2. Ye and co-workers [12] also found the similar phenomenon from WO_3 inverse opal. On the other hand, inverse opal structure provides high specific surface area and interconnected network. The former increases the density of active sites, while the latter has an advantage in rapid photo-charges and mass transfer. Therefore, inverse opal structures have great advantages in improving the photocatalytic activity of TiO_2.

For TiO_2 photocatalyst, many efforts have been made to widening the wavelength absorption into visible light range besides the attentions paid on improving the intrinsic absorption efficiency. Various chemical modification methods were applied to extend the absorption region of TiO_2 [3,4,13]. Currently, the combination of physical route (slow light effect of photonic crystal) and chemical routes (metal or non-metal doping, noble metal NP loading and p-n heterojunction) has proven to be a good way to improve the visible-light driven photocatalytic performance. For examples, Quan and co-workers [14] loaded Au nanoparticles on TiO_2 inverse opal and found that the slow light effect of TiO_2 porous matrix effectively enhanced the visible light harvesting ability of Au, leading to the improvement of visible-light driven photocatalytic activity of

* Corresponding author. Tel.: +86 021 64252062.
** Corresponding author at: Key Laboratory for Advanced Materials and Institute of Fine Chemicals, East China University of Science and Technology, 130 Meilong Road, Shanghai 200237, PR China. Tel.: +86 021 64252062; fax: +86 021 64252062.
E-mail addresses: wlz@ecust.edu.cn (L. Wang), jlzhang@ecust.edu.cn (J. Zhang).

http://dx.doi.org/10.1016/j.apcatb.2014.06.020
0926-3373/

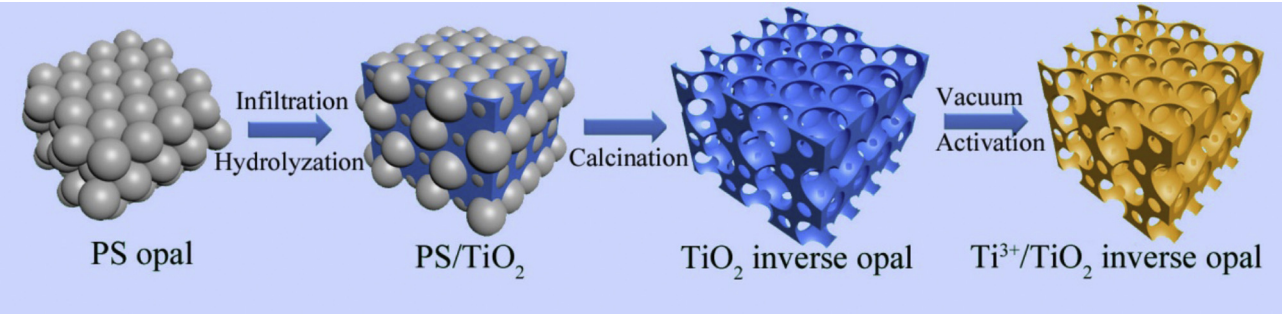

Fig. 1. Synthesis process of Ti^{3+} doped TiO_2 inverse opal structure.

Au-TiO_2 composite. Yang and co-workers [15] and Shang and co-worker [16] successfully improved the photocatalytic performance of TiO_2 in virtue of the synergistic effect of non-metal doping and slow light effect.

However, current chemical modification methods involving with the introduction of external species generally need harsh or troublesome preparation process. We recently found that a mild low-temperature vacuum treatment can effectively introduce Ti^{3+} into TiO_2 [17], where the light absorption range of TiO_2 was distinctly extended to visible range [18]. As a consequence, the visible light driven photocatalytic activities on water splitting and pollutant photodegradation were significantly improved.

In this study, TiO_2 inverse opals with different photonic stop bands were prepared via using different pore sized PS arrays as hard templates, and then Ti^{3+} and oxygen vacancies were introduced without damaging inverse opal structure by vacuum heating activation treatment (as shown in Fig. 1). This novel photocatalyst showed wide absorption spectrum and high efficient photocatalytic activity, which could be attributed to the synergistic effect of chemical Ti^{3+} self-doping and physical slow light effect. To our best knowledge, this is the first report on synergistic effect of photonic slow light effect and Ti^{3+} doping on enhancement of the visible light absorption ability and the photocatalytic activity.

2. Experimental

2.1. Materials

Tetrabutyl titanate (TBOT), potassium persulfate, lauryl sodium sulfate, ethanol, styrene, hydrochloric acid and acetylacetone were purchased from Sinopharm Chemical Reagent Company, Ltd.

2.2. Synthesis of PS colloidal crystal templates

Monodisperse PS spheres with different diameters were synthesized according to a previous report [19]. Typically, potassium persulfate (0.6 g) and lauryl sodium sulfate (0.45 g) were dissolved in the mixture of deionized water and ethanol at room temperature. In nitrogen atmosphere, the solution was heated to 344 K, and then styrene (36 mL) was added into the solution. The mixture was under mild continuous stirring for 19 h at 344 K. Finally, the obtained white colloidal suspension was filtered and stored in a narrow-mouth flask. The diameters of the PS spheres could be controlled by adjusting the amount of water and ethanol as follows (Table 1).

2.3. Fabrication of ordered PS arrays (solid)

Prepared PS colloidal suspension mentioned was transferred into petri dishes (fluid level height is about 15 mm). The petri dishes were kept in a 353 K oven until the liquid was dried out completely. Finally, the face-centered cubic PS array was obtained. According to the diameters of PS spheres, these samples were marked as PS-170, PS-265 and PS-355.

2.4. Fabrication of ordered PS arrays (film)

In order to characterize the spectra of PS arrays, PS-170, PS-265, PS-355 and PS-disordered films were prepared as follows: 400 μL prepared PS colloidal suspension was dispersed into 25 mL ultra pure water in a 25 mL beaker. Cleaned glass slide was immersed vertically into the beaker. The beaker was kept in a 353 K oven until the liquid was dried out completely. The obtained film was hexagonal close-packed PS arrays.

2.5. Preparation of TiO_2 inverse opals (solid)

In order to prepare ordered TiO_2 inverse opals, the forced impregnation method was used in infiltration process [20]. The prepared PS colloidal crystal templates were soaked completely in absolute methanol bath for 1 h. After that, these templates were taken out from the methanol bath and immediately immersed into tetrabutyl titanate. After vacuum impregnation for 10 h, the coated templates were removed from the tetrabutyl titanate bath and were dried and hydrolyzed in air at room temperature overnight. Then, the obtained samples were heated to 773 K at a rate of 1 °C/min and kept at this temperature for 4 h to remove the templates, giving TiO_2 with inverse opals structure. Finally, the samples were washed by water three times to remove the K_2SO_4, which generated from the potassium persulfate. Adjusting the diameters of the template PS spheres, titania inverse opals with different sizes could be obtained and then marked as T-170, T-265 and T-355. As reference samples, TiO_2 without any macropores was prepared by dropping TBOT in water and calcined in same condition and then marked as TiO_2-Blank. Mesoporous TiO_2 was prepared by mixing TBOT, hydrochloric acid, ethanol, water and F127 according to the molar ratios: 1:0.5:40:15:0.004, the solution was transferred to a petri dish and dried at 313 K for 48 h, after calcined at 673 K for 4 h white powder was obtained and marked as M-TiO_2.

2.6. Preparation of TiO_2 inverse opals (film)

In order to acquire the spectrum information of TiO_2 inverse opals, T-170, T-265 and T-355 films were prepared. Briefly, tetrabutyl titanate (5.6 mL) was added to a mixture of hydrochloric acid

Table 1
The amount of water and ethanol used in preparation of PS spheres.

Diameters of the PS spheres (nm)	Water (ml)	Ethanol (ml)
170	300	120
265	288	132
355	270	150

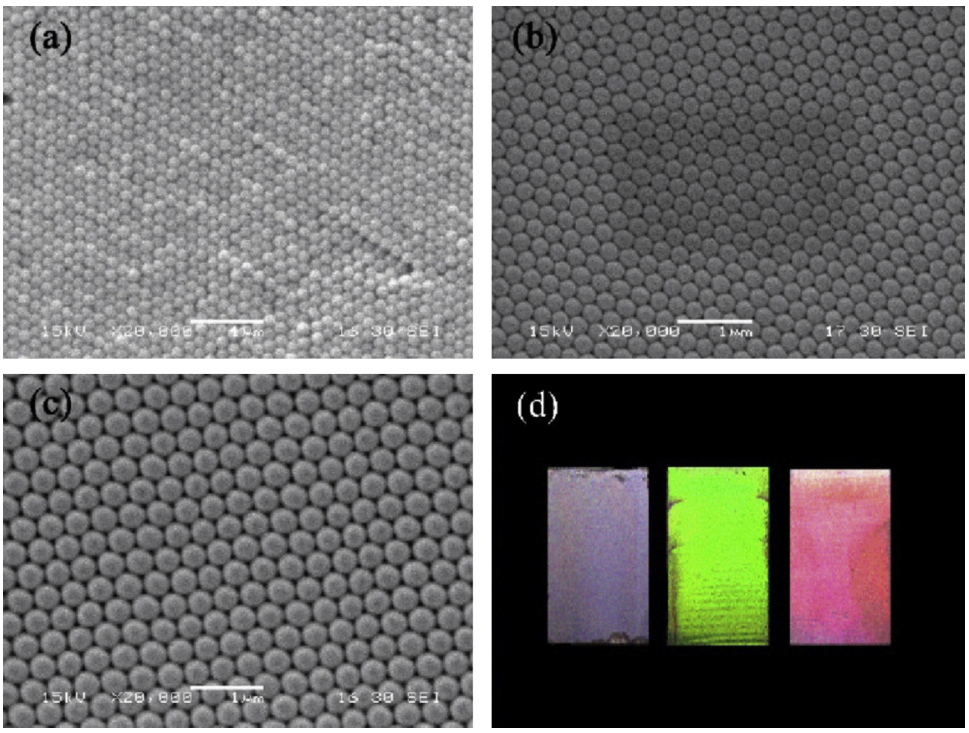

Fig. 2. SEM images of PS opals: (a) PS-170, (b) PS-265, and (c) PS-355. (d) Photograph of PS opal films PS-170, PS-265, and PS-355 from left to right.

(37%, 0.85 mL), acetylacetone (1 mL), ethanol (45 mL) and ultrapure water (4.6 mL) at room temperature under continuous stirring for 3 h. Spin coating process of the precursor solution on PS template films were carried out at 3000 r/min for 60 s. The coated slides were kept at 353 K for 48 h and then heated to 673 K for 4 h at a heating rate of 1 °C/min. As a result, TiO_2 inverse opals structure could be obtained.

2.7. Vacuum treatment of TiO_2 inverse opals (solid and film)

Vacuum treatment was carried out easily according to our previous work [17]. The TiO_2 inverse opals (solid and film) samples were heated to 573 K in vacuum for 3 h at a heating rate of 3 °C/min. After vacuum treatment, the samples were marked as V-M-TiO_2, V-T-160, V-T-265 and V-T-355.

2.8. Characterizations

In order to obtain the optical spectra of samples, UV–vis spectrophotometer (Shimadzu UV-2450) was used to analyze the absorption and transmission spectra of PS opal films and TiO_2 inverse opal films. Other characterizations were applied to analyze the solid samples. Field emission scanning electron microscopy (Hitachi S-3400) was used to observe the morphologies of the samples. X-ray photoelectron spectroscopy (XPS) was recorded with a PerkinElmer PHI 5000C ESCA system with Al Kα radiation operated at 250 W. BET surface area were obtained by surface area and porosity analyzer (Micromeritics ASAP 2020), and all samples were degassed in vacuum at 573 K for 8 h before measurements. X-ray powder diffraction (XRD) spectra were recorded on a Rigaku D/max 2550 VB/PC apparatus, operated at 40 kV and 30 mA. Electron paramagnetic resonance (EPR) spectra were recorded on Varian E-112 at room temperature to study the existence of Ti^{3+} and oxygen vacancies.

2.9. Light photocatalytic performance tests

The photocatalytic activities were evaluated by the photocatalytic degradation of acid orange 7 (AO7, 20 mg/L) under visible light and UV light irradiation, using a 500 W halogen lamp as the visible light source and high pressure mercury lamp as UV light source. In typical photocatalytic test, 0.07 g photocatalyst powders were added to 70 mL AO7 solution in a quartz tube. To establish an adsorption/desorption equilibrium, the suspensions were stirred magnetically in dark for 1 h before the irradiation. After some interval of time, 6 mL suspension were sampled and centrifuged to remove the remaining photocatalyst. The concentrations of the remaining AO7 solution were then analyzed by the UV–vis spectrophotometer.

3. Results and discussion

3.1. TiO_2 inverse opal structure and photonic stop band

The photonic stop bands of opal and inverse opal can be tuned by varying the size of PS spheres and calculated by the modified Bragg's law as the following equation:

$$\lambda = 2\sqrt{\frac{2}{3}}D\sqrt{n_m^2 f + n_{void}^2(1-f) - \sin^2\theta} \quad (1)$$

where λ is the wavelength of the photonic stop band, D is the diameter of the opal or the pore size of the inverse opal, n_m and n_{void} are the refractive index of host material and voids, f is the host phase volume percentage, which is taken as 0.74 for opal structure or 0.26 for inverse opal structure, and θ is the incident angle of light, which is 0° in this study.

Highly ordered opal templates of PS spheres with diameters of 170, 265 and 355 nm were prepared. Fig. 2a–c shows that PS spheres are hexagonal close-packed, and the spheres diameters are well controlled. As shown in Fig. 2d, the highly ordered opal films show brilliant colors, which can be explained by Bragg

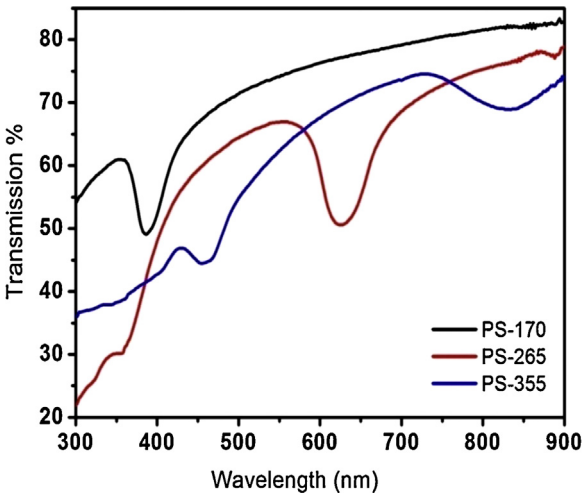

Fig. 3. Transmission spectra of the PS opal films with different sizes.

diffraction of visible light. In order to estimate the photonic stop bands of the PS films, transmission spectra of the opals films were measured as shown in Fig. 3. PS-170, PS-265 and PS-355 samples, respectively, show valley at 386 nm, 626 nm and 831 nm, respectively. These transmission valleys are attributed to the stop bands of highly ordered opal structure. The small valley at 490 nm observed from the curve of PS-355 might be caused by secondary diffraction, and similar phenomenon was also observed in previous work [12].

Highly ordered TiO_2 inverse opal structures were prepared via using PS opals as templates. The FESEM images of the TiO_2 inverse opal samples are shown in Fig. 4a–c. It is obviously that PS opals templates have been burned off, leaving interconnected macropores structures. The measured average pore sizes are about 130 ± 10, 180 ± 10, and 260 ± 10 nm, respectively. The diameters of inverse opals showed 25% shrinkage in comparison with sizes of the templates. Interconnected macropores should have an advantage in fast transportation of photogenerated electrons [21], which could improve the photocatalytic activity of the photocatalyst. It is known that the band gap of anatase is 3.2 eV and have no response to visible light. However, TiO_2 inverse opals show white, blue, and green color because of the different stop bands of various inverse opal structures (Fig. 4d).

To further prove the existence of the stop bands of these TiO_2 inverse opals, light absorption spectra were measured and shown in Fig. 5. As indicated by circles, a light absorption enhancement in specific region is observed in each titania inverse opal sample. To further confirm that the enhancement is generated by the stop band, a comparison data about the calculated and measured region of stop bands was listed in Table 2, where λ_c is the wavelength of photonic stop band calculated via Eq. (1), and λ_m is the wavelength of photonic stop band measured from Figs. 3 and 5. It is obvious that λ_c match well with λ_m for PS arrays, but they do not match so well for TiO_2 inverse opal arrays. This is because the incomplete infiltration of TiO_2 precursor so that f (host phase volume percentage) in Eq. (1) is smaller than 0.26. However, enhanced absorption regions are at the edge of photonic stop bands (Fig. 5), which is accord with slow light effect. Therefore, it is confirmed that absorption enhancement is caused by the slow light effect of TiO_2

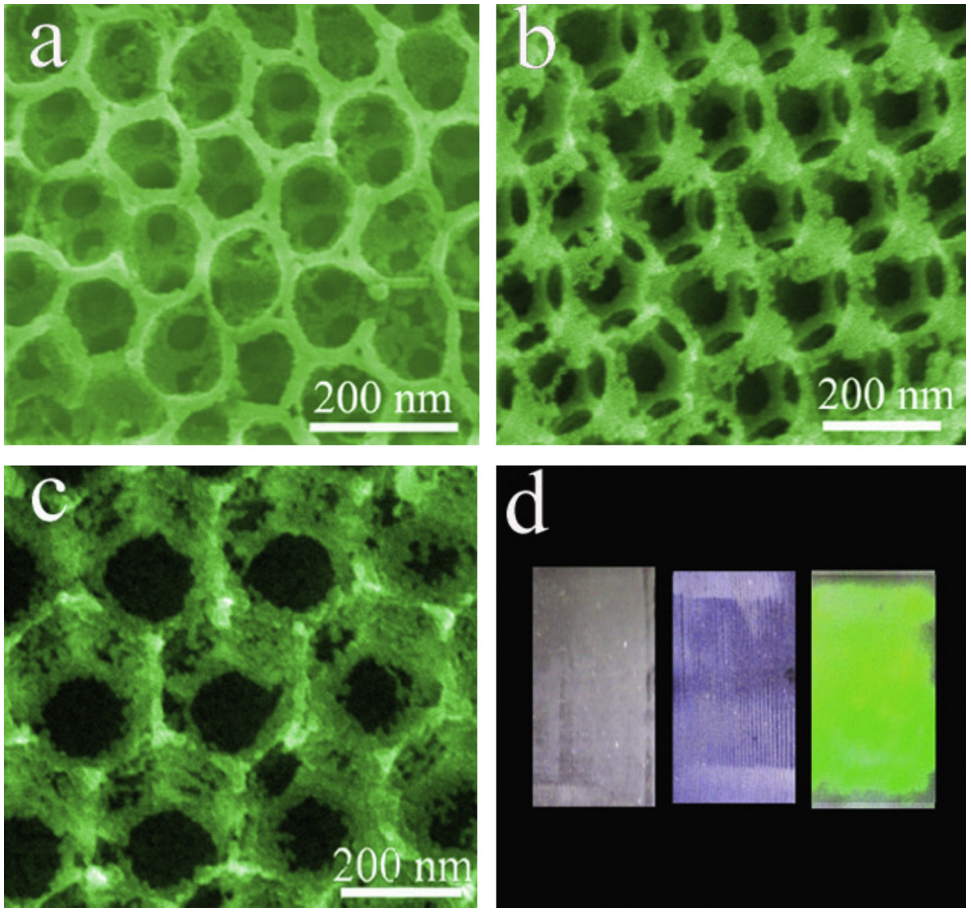

Fig. 4. (a–c) FESEM images of TiO_2 inverse opals, (a) T-170, (b) T-265, (c) T-355. (d) Photograph of TiO_2 inverse opal films T-170, T-265, and T-355 from left to right.

Table 2
Positions of stop bands of PS opals and TiO_2 inverse opals.

Samples	PS-170	PS-265	PS-355	T-170	T-265	T-355
Size (nm)	165(±5)	265(±5)	355(±5)	130(±10)	180(±10)	260(±10)
Refractive index	1.6	1.6	1.6	2.5	2.5	2.5
λ_c (nm)[a]	396	636	852	326	452	653
λ_m (nm)[b]	386	626	832	270	390	520

[a] Wavelength of photonic stop band calculated via Eq. (1).
[b] Wavelength of photonic stop band measured from Figs. 3 and 5.

Table 3
Crystal size and BET surface area of the samples.

Sample	TiO_2-Blank	M-TiO_2	T-170	T-265	T-355
Crystal size (nm)	42.4	–	18.1	18.2	20.3
BET surface area (m^2/g)	1.0	77	49.8	39.2	36.2

inverse opals and easily controlled by adjusting the diameters of PS templates.

3.2. Slow light effect on photocatalytic activity

XRD patterns of the samples were analyzed and shown in Fig. 6a. It is obvious that TiO_2 inverse opals still preserve anatase phase after calcination at 773 K, but TiO_2-Blank sample consists of anatase and rutile phase. Although high temperature tends to lead to a transformation from anatase to rutile, it seems that inverse opal structure could suppress the transformation tendency. To confirm this viewpoint, all of samples were further calcined in air at 700 °C for 2 h. Fig. 6b indicates that TiO_2-Blank almost completely transforms into rutile, but inverse opal samples show negligible transformation. Similar result has also been reported by Wiesner and co-workers [22]. Therefore, TiO_2 inverse opal structure tends to form anatase phase, whose photocatalytic activity is known to be much better than rutile phase. Furthermore, crystal sizes of the samples were calculated via Scherrer equation and listed in Table 3. The crystal sizes of TiO_2 inverse opal samples were about 20 nm, which was much smaller than that of TiO_2-Blank. This could be explained as follows: Close-packed PS array acts as backbone during the casting of TBOT, which can only be impregnated into the space between neighboring PS spheres, in situ hydrolyze and polymerize, thus the growth of titania particles is limited in the narrow space during calcination process. Small particle size could lead to higher specific surface area (Table 3) and more active sites, which should be beneficial for the improvement of photocatalytic activity.

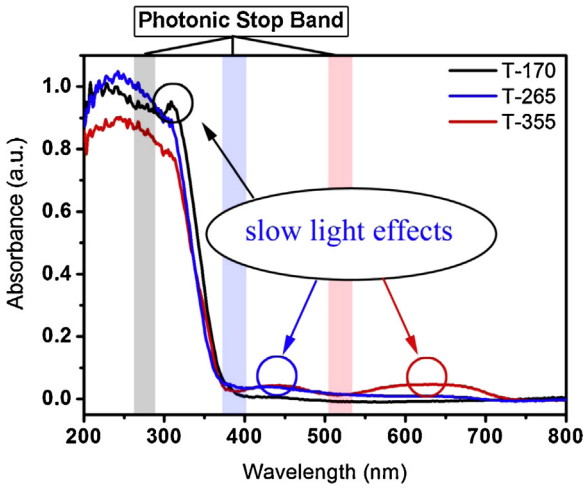

Fig. 5. UV-DRS spectra of TiO_2 inverse opal films.

To investigate the photocatalytic activity of titania inverse opals, photodegradation test of AO7 under UV light irradiation was performed and the results are shown in Fig. 7. Obviously, TiO_2-Blank sample shows the lowest photocatalytic activity, while T-170, T-265, and T-355 samples show much higher photocatalytic activity. This could be explained by the difference of crystal types and specific surface areas as illustrated above. Comparing with M-TiO_2 samples with similar surface area, inverse opal TiO_2 samples also show higher photocatalytic activity, indicating that light scattering property plays an important role in improving photocatalytic activity. Moreover, T-170 sample shows the highest photocatalytic activity among all three inverse opals, which could be attributed to the slow light effect of inverse opal structure. The stop band of T-170 is in the vicinity of 380 nm, which is near the characteristic absorption region of TiO_2. As a result, light harvesting improvement induced by the slow light effect enhances the UV light photocatalytic activity. In contrast, absorption enhancements are observed at 440 nm and 650 nm in the spectra of samples T-265 and T-355, but their photocatalytic activity are lower than sample T-170. This is because titania has no absorption in these regions, and the enhanced absorption cannot be used and makes no contribution to the photocatalytic activity. Moreover, the higher activity of sample T-355 than sample T-265 should be ascribed to the existence of enhanced scatting and absorption of second-order light near 400 nm. The above results confirm that slow light effect can actually improve the photocatalytic activity of TiO_2.

3.3. Ti^{3+} and oxygen vacancies induced by vacuum activation

Based on the above results and in consideration of the poor absorption ability of TiO_2 in the visible light region, we further applied the slow light effect for the improvement of the visible light responding ability of Ti^{3+} doped TiO_2 system. It has been reported that Ti^{3+} doping could extend the visible light absorption and improve the visible light photocatalytic activity [17]. We previously found that Ti^{3+} and oxygen vacancies can be generated easily in TiO_2 without damaging the morphology of the samples by mild vacuum heating treatment [17]. It has been found that during vacuum heating process, oxygen atoms might escape from the lattice of titania and generate oxygen vacancies and Ti^{3+}. Here, we adopted sample T-355 before and after vacuum treatment as models and applied electron paramagnetic resonance (EPR) spectra operated at room temperature without irradiation and O1s fine XPS for the characterization of oxygen vacancies and Ti^{3+}. As found from Fig. 8a, macroporous T-355 shows EPR signal at $g = 2.001$ while commercial TiO_2 (P25) shows no signal, and this signal should be ascribed to surface defects (probably electrons trapped on an oxygen vacancies). Serwicka [23] also observed this signal and attributed it to defect. It is believed that the macroporous inverse opal composed of nanocrystals and with high specific surface area could have abundant defects, which should be advantageous to the trapping of free electrons and lead to the formation of such characteristic signal. It is found that after vacuum treatment, two asymmetric peaks including a sharp peak at $g = 2.001$ and a wide peak around $g \approx 1.98$ arisen, which could be respectively attributed to the trapped electrons

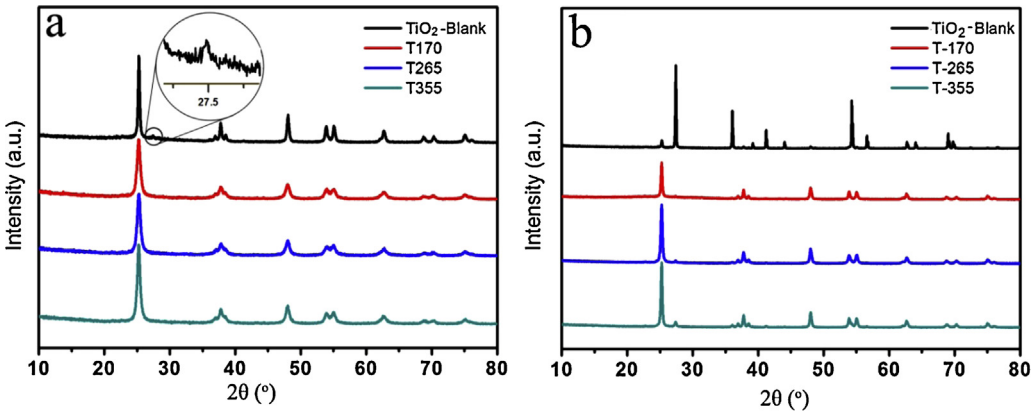

Fig. 6. XRD patterns of TiO_2-Blank and TiO_2 inverse opals (a) after 500 °C calcinations and (b) after 700 °C calcinations.

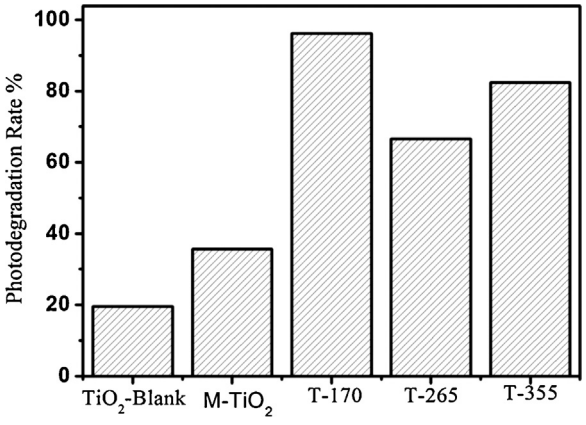

Fig. 7. Photodegradation of AO7 under UV light irradiation for 2 h.

by oxygen vacancies [18,23,24] and Ti^{3+} species [25–28]. On the other hand, the increased peak intensity at 532.5 eV in O1s fine XPS spectrum of sample V-T-355 observed from Fig. 8c further verifies the formation of oxygen vacancies after vacuum heating treatment [18]. However, Ti^{3+} signal was not detected by XPS analysis. It is known that compared with oxygen vacancy, Ti^{3+} in the surface layer is highly reactive with H_2O and O_2 molecules when they are exposed in air, leading to the hard detection of Ti^{3+} by XPS. Therefore, the above results from EPR and XPS confirm the existence of Ti^{3+} in the bulk of vacuum activated TiO_2 inverse opal.

To compare the quantity of Ti^{3+} and oxygen vacancy, EPR spectra of the samples were presented in Fig. 8b. It can be found that the spectra of all samples showed similar intensity, indicating the quantity of Ti^{3+} and oxygen vacancy in the samples are almost same.

3.4. Synergistic effect of inverse opal structure and vacuum activation

Our previous work found that oxygen vacancies and Ti^{3+} could narrow the band gap of TiO_2 and induce visible light harvesting. Similar phenomenon was observed in this work, visible light response of TiO_2 inverse opal films were improved after vacuum heating treatment as shown in Fig. 9. T-170 film shows no visible light absorption and V-T-170 film can absorb visible light with wavelength shorter than 550 nm, and the absorption is improved greatly for V-T-265 film. It is noteworthy that the light absorption of V-T-355 film is extended to 750 nm, meaning that it can absorb entire visible light region. Taking V-T-355 sample as an example, the photonic stop band of its inverse opal structure was in visible region, and the light around its edge could be absorbed because of slow light effect. On the other hand, vacuum activation generates oxygen vacancies and Ti^{3+}, which narrows the band gap of titania, so that the photocatalyst could further absorb visible light. As discussed above, the effect of difference in Ti^{3+} species quantity can be rule out (Fig. 8b). Therefore, the enhanced absorption ability was attributed to the synergistic effect of slow light in visible region and Ti^{3+} doping.

To investigate whether the above synergistic effect on improving the visible light absorption could be used to improve the visible-light driven photocatalytic activity, photodegradation test on AO7 were performed, and the results are shown in Fig. 10. It is obvious that M-TiO_2 sample shows the lowest photocatalytic activity, and its photocatalytic activity is improved after

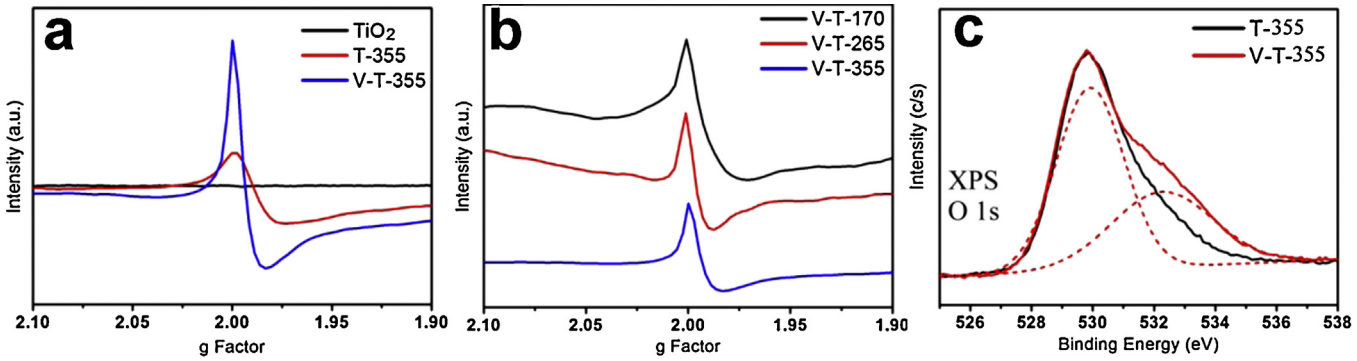

Fig. 8. EPR spectra of T-355, V-T-355, and commercial TiO_2 (P25) recorded at room temperature in dark (a), EPR spectra of V-T-170, V-T-265 and V-T-355 (b), and XPS O1s fine spectra of T-355 and V-T-355 (c).

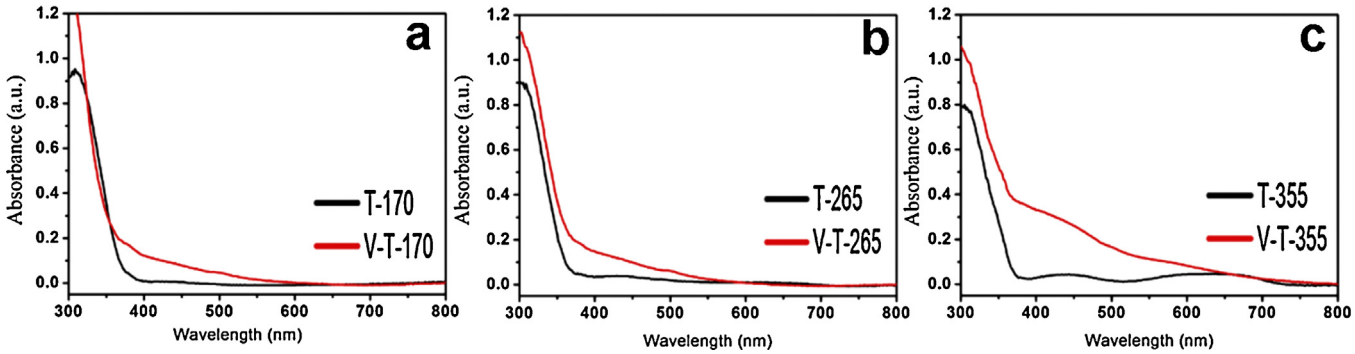

Fig. 9. UV-DRS spectra of TiO_2 inverse opals films before and after vacuum heating treatment. (a) T-170 and V-T-170; (b) T-265 and V-T-265 and (c) T-355 and V-T-355.

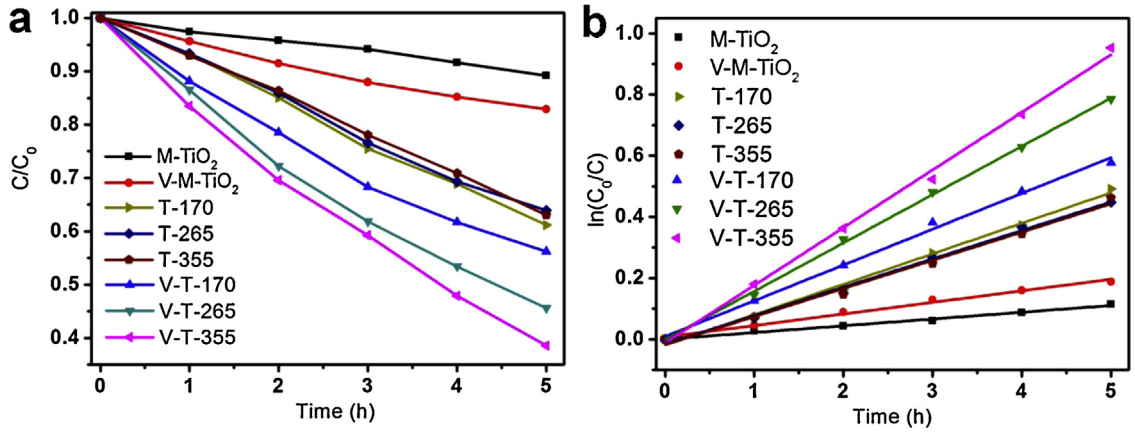

Fig. 10. (a) Photodegradation of AO7 under visible light irradiation and (b) kinetics of AO7 Photodegradation under visible light irradiation.

vacuum activation, indicating Ti^{3+} and oxygen vacancies can actually develop visible light photocatalytic activity. On the other hand, T-170, T-265, and T-355 samples show similar photocatalytic activity. Although they show enhanced absorption in visible region because of their inverse opal structures, titania still cannot be excited because of its wide band gap, resulting in no difference between their photocatalytic activities. After vacuum activation, the band gap of titania is narrowed because of the presence of Ti^{3+} and oxygen vacancies. Enhanced light harvesting caused by inverse opal structures could be applied to generate photoelectrons and photoholes, so that the photocatalytic activity could be improved further. V-T-355 shows most wide absorption in visible light region so that its photocatalytic activity is the highest. Therefore, it is confirmed that the synergistic effect on visible light harvesting of inverse opal structure and vacuum activation can actually be applied to enhance photocatalytic activity.

Based on the above studies, the mechanism of synergistic effect is explained and illustrated in Fig. 11. As a physical way for light absorption enhancement, adopting of inverse opal structure can help to absorb lights near the photonic stop band of inverse opal. Ultraviolet light at 370 nm can be absorbed by T-170 sample because of slow light effect, and titania is excited by light in this region, so it can be in full use to achieve better photocatalysis efficiency. As a result, T-170 shows best UV photocatalytic activity. In a similar way, T-355 sample absorbs more visible light because of slow light effect. On the other hand, the band gap of titania is narrowed by Ti^{3+} doping so that it can make use of visible light. Thus, V-T-355 sample presents best visible light photocatalytic activity. As a contrast, the samples without visible region stop band or Ti^{3+} doping show lower photocatalytic activity because the synergistic effect can not be achieved in those samples.

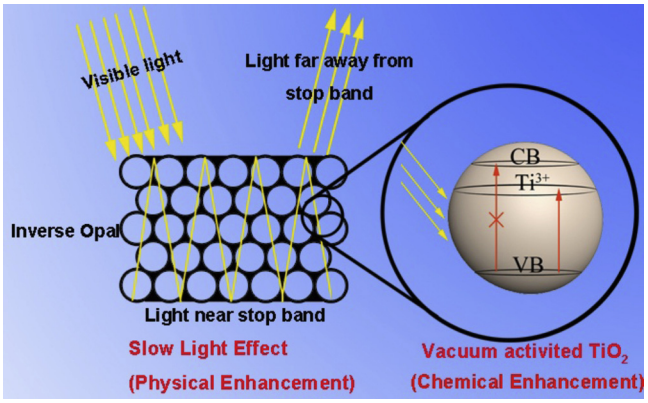

Fig. 11. Synergistic effect of slow light effect (physical enhancement) and vacuum activation (chemical enhancement).

4. Conclusions

In summary, Ti^{3+} doped TiO_2 inverse opal photocatalyst was prepared by a simple and mild vacuum heating treatment for TiO_2 inverse opal. This novel photocatalyst showed synergistically enhanced visible light harvesting ability due to the slow light effect and Ti^{3+} doping. The combination of highly porous structure and good light harvesting ability endowed the TiO_2 photocatalyst excellent photocatalytic performance. We hope our research could provide a good model and designing way for highly efficient solar light driven photocatalyst.

Acknowledgments

This work has been supported by the National Natural Science Foundation of China (21173077, 21377038 and 21237003), the National Basic Research Program of China (973 Program, 2013CB632403), the Project of International Cooperation of the Ministry of Science and Technology of China (No. 2011DFA50530); Science and Technology Commission of Shanghai Municipality (12230705000, 12XD1402200), the Research Fund for the Doctoral Program of Higher Education (20120074130001) and the Fundamental Research Funds for the Central Universities.

References

[1] A. Fujishima, K. Honda, Nature 238 (1972) 37–38.
[2] M. Xing, J. Zhang, F. Chen, J. Phys. Chem. C 113 (2009) 12848–12853.
[3] M. Xing, D. Qi, J. Zhang, F. Chen, Chem.-Eur. J. 17 (2011) 11432–11436.
[4] Y. Cong, J. Zhang, F. Chen, M. Anpo, J. Phys. Chem. C 111 (2007) 6976–6982.
[5] Y. Wu, H. Liu, J. Zhang, F. Chen, J. Phys. Chem. C 113 (2009) 14689–14695.
[6] M. Takeuchi, M. Matsuoka, M. Anpo, Res. Chem. Intermediat. 38 (2012) 1261–1277.
[7] S. Sakthivel, H. Kisch, Angew. Chem. Int. Ed. 42 (2003) 4908–4911.
[8] A. Stein, B.E. Wilson, S.G. Rudisill, Chem. Soc. Rev. 42 (2013) 2763–2803.
[9] T.F. Krauss, R.M.D.L. Rue, S. Brand, Nature 383 (1996) 699–702.
[10] C. Cheng, S.K. Karuturi, L. Liu, J. Liu, H. Li, L.T. Su, A.I.Y. Tok, H.J. Fan, Small 8 (2012) 37–42.
[11] J.I.L. Chen, G. von Freymann, S.Y. Choi, V. Kitaev, G.A. Ozin, Adv. Mater. 18 (2006) 1915–1919.
[12] X. Chen, J. Ye, S. Ouyang, T. Kako, Z. Li, Z. Zou, ACS Nano 5 (2011) 4310–4318.
[13] X. Chen, S.S. Mao, Chem. Rev. 107 (2007) 2891–2959.
[14] Y. Lu, H. Yu, S. Chen, X. Quan, H. Zhao, Environ. Sci. Technol. 46 (2012) 1724–1730.
[15] J. Xu, B. Yang, M. Wu, Z. Fu, Y. Lv, Y. Zhao, J. Phys. Chem. C 114 (2010) 15251–15259.
[16] Q. Li, J.K. Shang, J. Am. Ceram. Soc. 91 (2008) 660–663.
[17] M. Xing, J. Zhang, F. Chen, B. Tian, Chem. Commun. 47 (2011) 4947–4949.
[18] T. Xia, W. Zhang, J.B. Murowchick, G. Liu, X. Chen, Adv. Energy Mater. 3 (2013) 1516–1523.
[19] N. Yu, C. Liu, Y. Shan, K. Chen, J. Qingdao Univ. Sci. Technol. 31 (2010) 351–360.
[20] X. Chen, Z. Li, J. Ye, Z. Zou, Chem. Mater. 22 (2010) 3583–3585.
[21] B. Mandlmeier, J.M. Szeifert, D. Fattakhova-Rohlfing, H. Amenitsch, T. Bein, J. Am. Chem. Soc. 133 (2011) 17274–17282.
[22] M.C. Orilall, N.M. Abrams, J. Lee, F.J. DiSalvo, U. Wiesner, J. Am. Chem. Soc. 130 (2008) 8882–8883.
[23] E. Serwicka, Colloids Surf. 13 (1985) 287–293.
[24] V.N. Kuznetsov, N. Serpone, J. Phys. Chem. C 113 (2009) 15110–15123.
[25] I. Nakamura, N. Negishi, S. Kutsuna, T. Ihara, S. Sugihara, K. Takeuchi, J. Mol. Catal. A: Chem. 161 (2000) 205–212.
[26] R.F. Howe, M. Gratzel, J. Phys. Chem. 89 (1985) 4495–4499.
[27] J. Cho, J. Seo, J.-K. Lee, H. Zhang, R. Lamb, Physica B 404 (2009) 127–130.
[28] F. Zuo, L. Wang, T. Wu, Z. Zhang, D. Borchardt, P. Feng, J. Am. Chem. Soc. 132 (2010) 11856–11857.